TECHNICAL DIVISION
SAVANNAH RIVER LABORATORY

WSRC-RP--89-635

DE93 003260

Distribution:

L. M. Papouchado, 703-A

J. B. Mellen, 704-S (5)   D. C. Nichols, 704-S (5)
R. M. Harral, 704-S   H. H. Elder, 704-S
J. A. Jentilucci, 704-S   D. C. Witt, 704-S
B. K. Sanders, 704-11S   W. T. Davis, 704-1'.S
R. G. Baxter, 704-S   K. O. Darden, 704-S
A. L. Applewhite, 704-S   P. D. Guidotti, 704-11S
G. F. Rabon, 704-30S   G. A. Griffin, 704-16S
S. L. Goudelock, 704-27S

D. L. McIntosh, 773-A   R. M. Wallace, 773-A
J. R. Knight, 773-A   G. T. Wright, 773-A
J. A. Stone, 773-A   M. D. Boersma, 773-41A
M. J. Plodinec, 773-A   W. W. F. Yau, 773-A
D. F. Bickford, 773-A   C. M. Jantzen, 773-A
C. T. Randall, 704-T   L. F. Landon, 704-T
J. T. Carter, 704-1T   L. M. Lee, 704-T
R. E. Edwards, 704-1T   I. G. Choi, 704-1T
LSEG, 704-1T (13)

SRL Records, 773-A (4)

August 25, 1989

MEMORANDUM

To: Distribution

From: A. S. Choi, 704-1T

Re: SGM Freeze/Restart Report

An error has occurred in the document number of the previously
issued report on SGM Freeze/Restart Campaign (WSRC-RP-89-635).
Please replace it with the attached report (WSRC-RP-89-634). No
changes have been made to any of its contents.

Westinghouse
Savannah River Company

CC:
D. C. Nichols, 704-S (5)
R. M. Harral, 704-S
H. H. Elder, 704-S
J. A. Gentilucci, 704-S
B. K. Sanders, 704-11S
W. T. Davis, 704-12S
D. C. Witt, 704-S
R. G. Baxter, 704-S
K. O. Darden, 704-S
A. L. Applewhite, 704-S
P. D. Guidotti, 704-11S
G. F. Rabon, 704-30S
G. A. Griffin, 704-16S
S. L. Goudelock, 704-27S
SRL Records   (4)

July 31, 1989

L. M. PAPOUCHADO, MANAGER WASTE MANAGEMENT
WESTINGHOUSE SAVANNAH RIVER COMPANY

ATTENTION: J. B. MELLEN, 704-S (5)

FREEZE AND RESTART
OF THE DWPF SCALE GLASS MELTER (U)

The attached memorandum (WSRC-RP-89-635) discusses the results of the last DWPF Scale Glass Melter campaign. The primary objectives were to characterize the transient melter operations and to examine the relative startup capability of the DWPF Melter on a theoretical basis. Many of the results are directly applicable to the DWPF.

J. R. KNIGHT, RESEARCH MANAGER
DEFENSE WASTE PROCESSING TECHNOLOGY DIVISION

J. R. Knight, 773-A
Authorized Derivative Classifier

OSR 25-82-W(4-89)

M E M O R A N D U M

To: C. T. Randall, 704-T

From: A. S. Choi, 704-1T $\mathcal{ASC}$
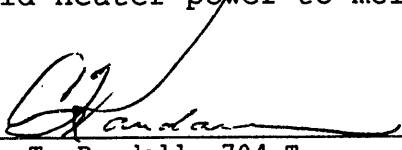
FREEZE AND RESTART
OF THE DWPF SCALE GLASS MELTER (U)

SUMMARY

After over two years of successful demonstration of many design and
operating concepts of the DWPF Melter system, the last Scale Glass
Melter campaign was initiated on 6/9/88 and consisted of two parts;
(1) simulation of noble metal buildup and (2) freeze and subsequent
restart of the melter under various scenarios. The objectives were
to simulate a prolonged power loss to major heating elements and to
examine the characteristics of transient melter operations during a
startup with a limited supply of lid heat.

Experimental results indicate that in case of a total power loss to
the lower electrodes such as due to noble metal deposition, spinel
crystals will begin to form in the SRL 165 composite waste glass
pool in 24 hours. The total lid heater power required to initiate
joule heating was the same as that during slurry-feeding. Results
of a radiative heat transfer analysis in the plenum indicate that
under the identical operating conditions, the startup capabilities
of the SGM and the DWPF Melter are quite similar, despite a greater
lid heater power to melt surface area ratio in the DWPF Melter.

C. T. Randall, 704-T
Authorized Derivative Classifier

SUMMARY OF CONCLUSIONS

1. The startup temperature for joule heating of the DWPF startup glass is about 25°C higher than that of the SGM Freeze/Restart glass which is less viscous and less electrically resistant than the former.

2. In case of a total power loss to the lower electrodes, the melt which is initially at 1075°C in the lower regions of the pool will reach the DWPF operating limit of 200 poise at 950°C in 12 hours. Spinel crystals will then begin to form near the bottom of the SRL 165 composite waste glass pool 12 hours after the limiting viscosity range is reached.

3. The power supply during radiant heating is limited by the hot spot temperature on the lid heaters. During slurry-feeding, the lid heater surface temperature becomes the limiting factor.

4. At the onset of joule heating, the total lid heater power flux was 10.5 KW/ft^2 of melt surface area, which is a typical value required during slurry-feeding to maintain the design melt rate of 100 pph.

5. Regardless of whether it is a startup with fresh frit or frozen glass, melt temperatures between 630 and 640°C at the midpoint of a electrode front face appear to be a good criterion for when to attempt joule heating.

6. The riser channel has no effect on the overall thermal behevior of the melt pool during steady state or transient operations.

7. The startup capability of the DWPF Melter is at best marginally better than that of the SGM, and this is partly attributed to a larger conductive heat loss both above and below the melt line in the former.

8. During the radiant heating period, 25% of the total radiative heat flux incident on the glass surface comes directly from the lid heaters, while the corresponding lid heater contribution in the DWPF Melter is 35%. In each melter, the remaining incident flux comes from the refractory walls and the lid.

9. During the radiant heating period, 98% of the total radiation incident on the glass surface is emitted back into the plenum, resulting in a net influx ranging from 80 to 100 W/ft^2 of melt surface area in both SGM and DWPF Melter.

TABLE OF CONTENTS

LIST OF FIGURES

LIST OF TABLES

INTRODUCTION

After the post SGM-10 inspection was completed, the following test plans for the final Scale Glass Melter (SGM) campaign were adopted based upon SRL/SRP discussions:

    I. Simulation of the lower electrode current bypassing through the conductive noble metal layer formed on the melter floor.

    II. Freeze and subsequent restart of the melter under various scenarios.

In Test I, the lower electrode power was turned off in order to simulate complete bypassing of its current through the metal layer. The subsequent decrease in melt temperatures, especially in the lower regions of the pool, was carefully monitored. The duration of test was determined in such a way that the crystal formation both in the melt pool and in the dump valve channel was minimized.

Test II was recognized as the major effort of the campaign, and its objective was to examine the startup capability of the DWPF Melter based on SGM campaign data. The melt pool was first cooled below 500°C to simulate a prolonged power loss to the major heating units such as the electrodes due to operational difficulties. Using only the radiant heat from the lid heaters, the frozen glass matrix was then heated progressively to determine the nominal lid heater power required to raise the glass temperatures high enough to establish joule heating in the upper regions of the pool.

The startup capability of the DWPF Melter was compared to that of the SGM on a theoretical basis by calculating the transient glass temperatures in each melter during radiant heating. The analysis involved calculation of the net radiative heat flux into the glass by considering both melter design and operating characteristics.

A simulation study of the transient thermal behavior of the glass matrix was initiated concurrently with the Freeze/Restart campaign during 1988 at Pacific Northwest Laboratory under a contract with SRL. A transient, 3-D finite difference code, called TEMPEST, was used in the simulation, and the full results have been documented elsewhere.[1]

Scale Glass Melter Description

The Scale Glass Melter, shown in Figure 1, is a 2/3-linear-scale of the current DWPF design, and both melters are slurry-fed. The SGM was designed to produce glass at 100 pph, compared with 228 pph for the DWPF Melter. A detailed description of design comparisions of the two melters has been given elsewhere,[2] and only the key design features of the SGM heating systems are mentioned briefly here.

There are two horizontal lid heater units in an over-and-under configuration, and each unit is configured with two elements in series for a total of four heater tubes in the plenum. Each unit
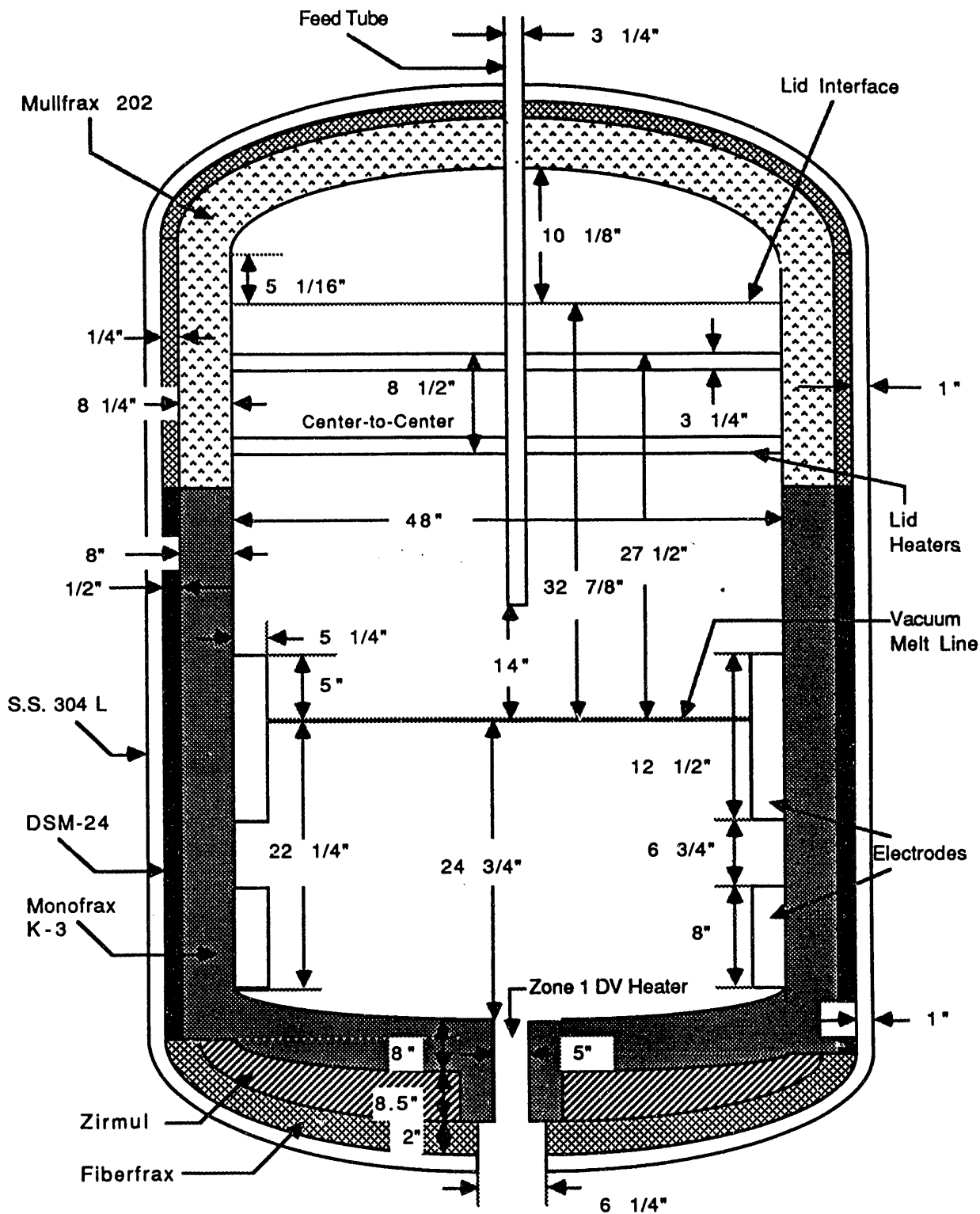
FIGURE 1. Cross-Sectional View of the SGM Cut along Symmetry Plane of Electrodes (not to scale).

has its own power supply and a single loop PID controller. Before joule heating is established during melter startup, these heaters are the primary source of heat. The lid heater surface temperature is normally set at 950°C during slurry feeding to give 120 KW total power. The ratio of nominal lid heater power to melt surface area in the SGM is 76% of that in the DWPF Melter. Based on this ratio, the DWPF Melter should have a greater startup capability and higher boil-off and melt rates than the SGM.[2]

Energy balance calculations[3] showed that 45-60% of the total heat transferred to the cold cap was due to the radiant heat from the lid heaters and the refractory walls in the plenum. Consequently, the remainder should enter the cold cap via joule heat. Two pairs of diametrically opposed Inconel 690 electrodes enter the melter cavity in an over-and-under split configuration, and they provide the melt pool with 90 KW power to maintain the glass temperatures between 1050°C and 1150°C. Each pair has its own power supply with a cascade temperature control loop to allow independent diversion of power. The electrode power density is almost identical in each melter at ~12 KW/ft^2 of electrode surface, and the current density is limited to 5 A/in^2 of electrode surface to prevent overheating of the metal.[2]

Both the riser and pour spout channels are wrapped independently with the serpentine resistance heaters to keep the glass stream fluid during pouring. The normal operating temperature for each heater is set at 1100°C. The inside diameter of the riser channel is 2.67" in the SGM and 4" in the DWPF Melter, and the velocity of the glass stream in the channel is identical at 0.27 ft/min for the two melters. The dump valve in the SGM consists of 3 heater zones, compared with 5 zones in the DWPF Melter. The uppermost zone 1 heater is closest to the melt pool and provides 600 W during normal operations at a setpoint of 1000°C in the SGM. Zone 2 and 3 heaters are energized only during draining operations.

EXPERIMENTAL RESULTS AND DISCUSSION

The experimental procedures for Tests I and II are described in Job Plan #675-T-88-5-1 and #675-T-88-6-(1-4), respectively. All of the experimental observations having an operational significance in the DWPF are discussed next in chronological order.

The melt temperatures were measured in two thermowells, called East and West. Both thermowells were vertically suspended into the melt pool at 19.5" from the center axis and 180° apart from each other. In the East thermowell, there were eight type K thermocouples, each positioned at 1.5" through 20.75" below the vacuum melt line, and the distance between two adjacent thermocouples was 2.75". In the West thermowell, there were three thermocouple positions, at 6.75", 13.75", and 20.25" below the vacuum melt line. However, unlike in the East thermowell, two type B thermocouples were inserted at each depth, side-by-side less than 1" apart, thus allowing the degree of local temperature fluctuations to be measured.

Comparison of Startup Glass Properties

After the SGM-10 campaign was completed, 500 lbs of DWPF startup frit was added to the melt inventory. The final melt composition for Tests I & II (SGM Freeze/Restart) is compared in Table A.1 in Appendix with those of other startup frits. Sharp-Schurtz measured the viscosities of glass samples collected during draining at the end of Test II, and the Fulcher-Tammann constants for all types of startup glasses are given in Table A.2 in Appendix.[4]

The Sharp-Schurtz viscosities for both SGM Freeze/Restart (F/R) and DWPF startup glasses are plotted in Figure 2 on a semi-log$_{10}$ scale, and they are shown to be within the operating limits for the DWPF reference waste glass. The SGM F/R glass is also shown to be less viscous than the DWPF startup glass mainly due to its lower SiO_2 and higher B_2O_3 contents. Therefore, after the joule heating is established, the convective mixing is expected to be more efficient in the SGM F/R glass than in the DWPF startup glass.

An X-ray diffraction analysis also revealed that the SGM F/R glass contained spinels ($NiFe_2O_4$-$MgFeAlO_4$) and SiO_2.[4] This was expected because the melt pool was maintained at low temperatures for an extended period of time during both tests. In a dilute suspension
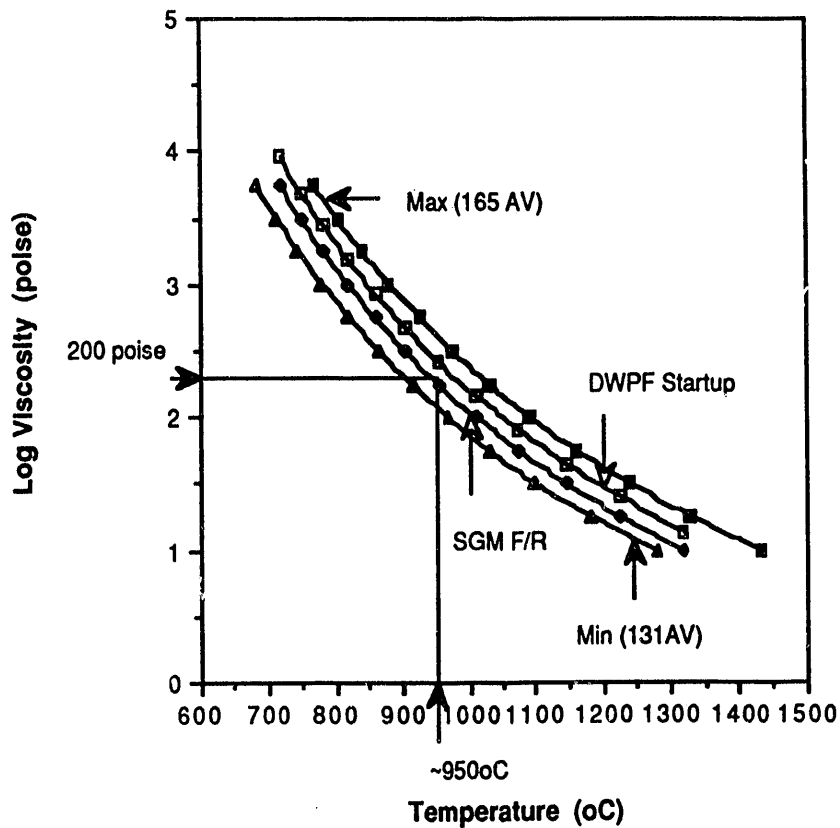
FIGURE 2. Comparison of Startup Glass Viscosities.

of non-agglomerating particles, the apparent viscosity has a linear or quadratic dependence on the volume fraction of solid particles.[5] Hence, under the normal conditions, the viscosities of the SGM F/R glass could have been a little lower than those shown in Figure 2.

No measurements on the electrical resistivity have been made as yet for the startup glasses. In order to assess the relative startup capabilities based on glass resistivity, the following correlation was used to estimate the unknown resistivities:

$$\eta = 2.66 \times \rho^{2.06} \tag{1}$$

where ρ is the resistivity in Ω-cm, and η is in poise. It is noted that Eq.1 was derived by correlating the Sharp-Schurtz viscosity data against the Corning Glass Works resistivity data.[6]

The resistivities for both startup glasses are shown in Figure 3 to be within the DWPF operating limits, and the DWPF startup glass is seen to be more resistive than the SGM F/R glass. At the onset of joule heating during Test II, the glass temperature near the top of the upper electrodes was 695°C. The resistivity of SGM F/R glass at 700°C is estimated from Figure 3 to be ~49 Ω-cm.
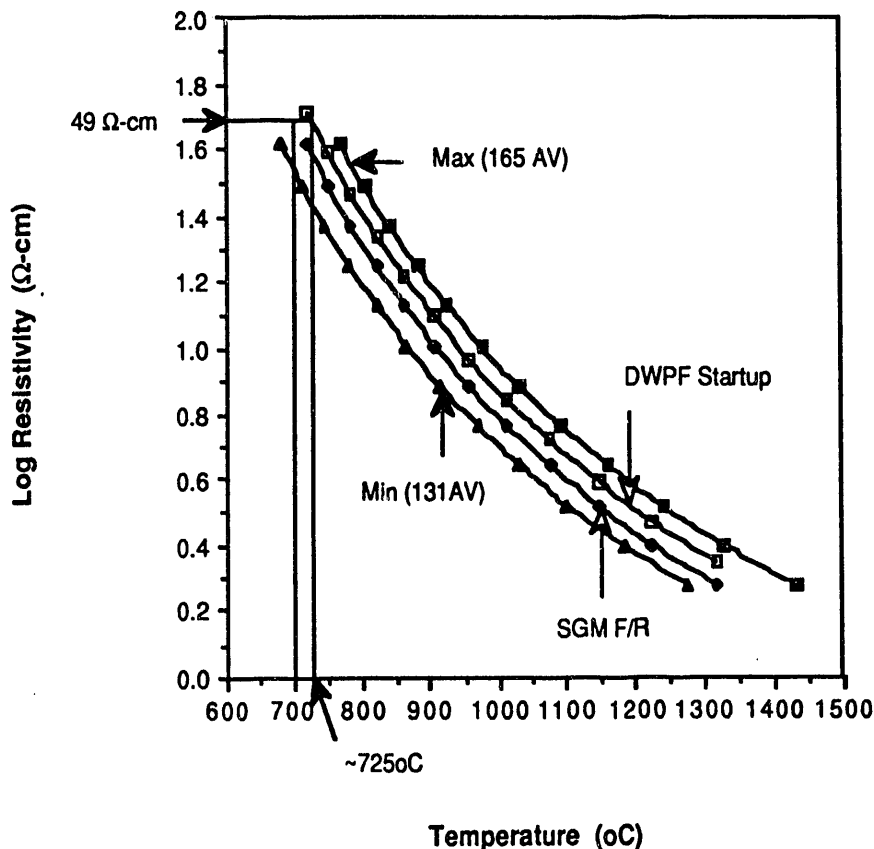
FIGURE 3. Comparison of Startup Glass Resistivities.

Figure 3 also shows that the startup temperature for joule heating is ~25°C higher for the DWPF startup glass. Given that the maximum allowable rate of glass temperature rise is set at 10°C/hr, this is equivalent to at least 2-1/2 additional hours of radiant heating, provided that the applied electrode potentials are the same across the two glasses. During an earlier restart attempt,[7] it took about 7 days to heat up a fresh charge of DWPF startup frit from ambient temperature to 720°C at the top of the lower electrodes when joule heating was established. As predicted, the startup temperature for joule heating was indeed 25°C higher for the DWPF startup frit.

Test I. Simulation of Noble Metal Buildup

At 11:00 am on 6/9/88, the lower electrode power was cut off, and this point was marked as time zero. Initially, the upper and lower electrodes were supplying 15 KW and 80 KW, respectively, and the upper electrode power was increased to 75 KW at time zero in order to prevent any excessive temperature drop. As shown in Figure 2, the lower temperature limit was set at 950°C to remain below the maximum DWPF operating viscosity of 200 poise during power outage.[8] Throughout Test I, the upper and lower lid heaters were supplying 30 KW each, and the vapor space temperature remained at ~870°C.

The vertical melt temperature profiles during Test I are shown in Figure 4. The lowest melt temperature was measured at the deepest thermocouple position, 20.75" below the melt line, and reached the lower temperature limit in less than 13 hours. The average rate of temperature decrease at this depth was 10°C/hr during this period, and it was decreased to 2.5°C/hr during next 20 hours. The lower electrodes were turned on to its full power of 80 KW at the 33 hour mark, and the lower melt temperatures began to rise instantaneously and reached close to their initial values in less than 10 hours.

The temperature drops measured during the power outage are plotted in Figure 5 against the melt depth. Two thermally distinct regions are seen to develop in the melt pool around the 11" point from the melt surface, which is precisely the midpoint between the upper and lower electrodes. The melt temperatures above this point exhibited little change or actual increases due to the increase in the upper electrode power and, below it, all the melt temperatures decreased during power outage. As expected, the extent of the temperature drop increased with increasing melt depth.

Summing up the results of Test I, it may be concluded that in the worst case of total power loss to the lower electrodes, the melt near the floor will reach the limiting viscosity of 200 poise at 950°C in about 12 hours even with the full upper electrode power. During the next 12 hours, the melt temperatures will drop to 920°C. As illustrated in Figure 6, line XY represents the locus of 12 hour isothermal annealing points between 950 and 920°C, and it is seen that the envelope for spinel formation intersects line XY near its midpoint. Therefore, it appears that spinel crystals will begin to form in the lower regions of the pool of SRL 165 composite waste glass about 12 hours after the limiting viscosity range is reached.
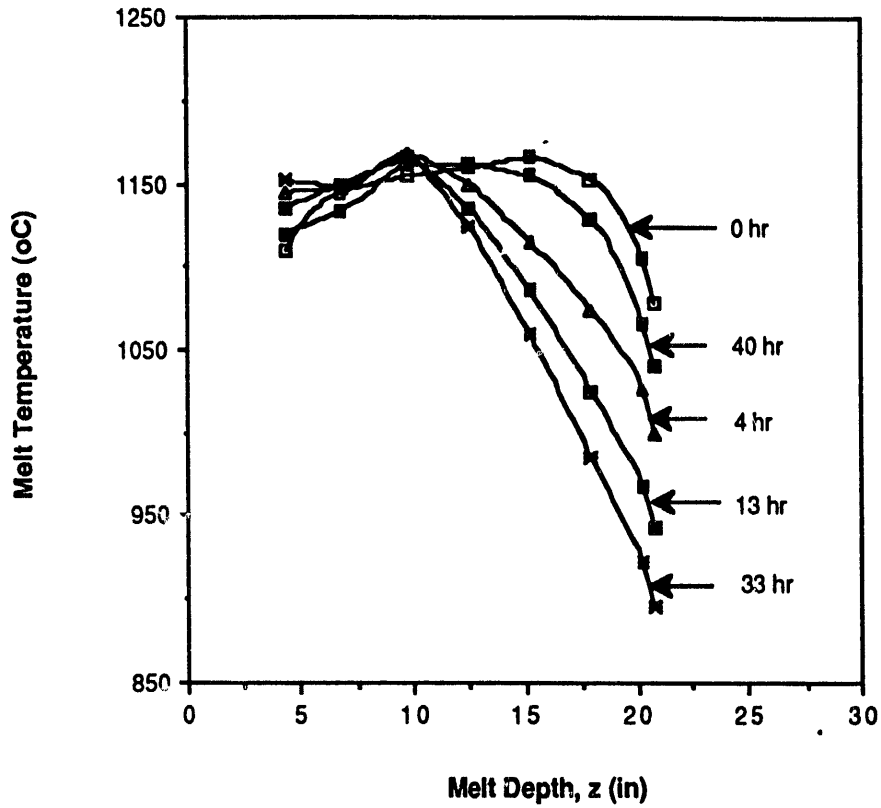
FIGURE 4. Time Variation of Vertical Temperature Profiles.

$y = 118.4014 - 14.8504x \quad R = 0.97$
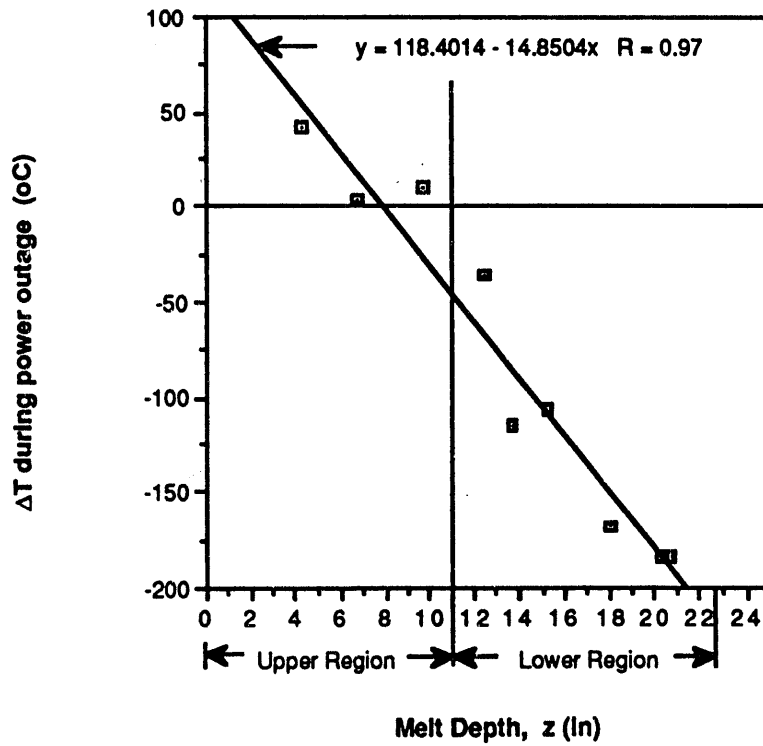
FIGURE 5. Temperature Drop during Test I.

It should be noted that both Test I and II were run entirely under
idling conditions. However, since the thermal characteristics of
the melt near the melter floor are likely to remain the same during
idling or feeding, the threshold point of spinel formation during
slurry-feeding is still expected to be about 24 hours after the
total power loss is initiated.
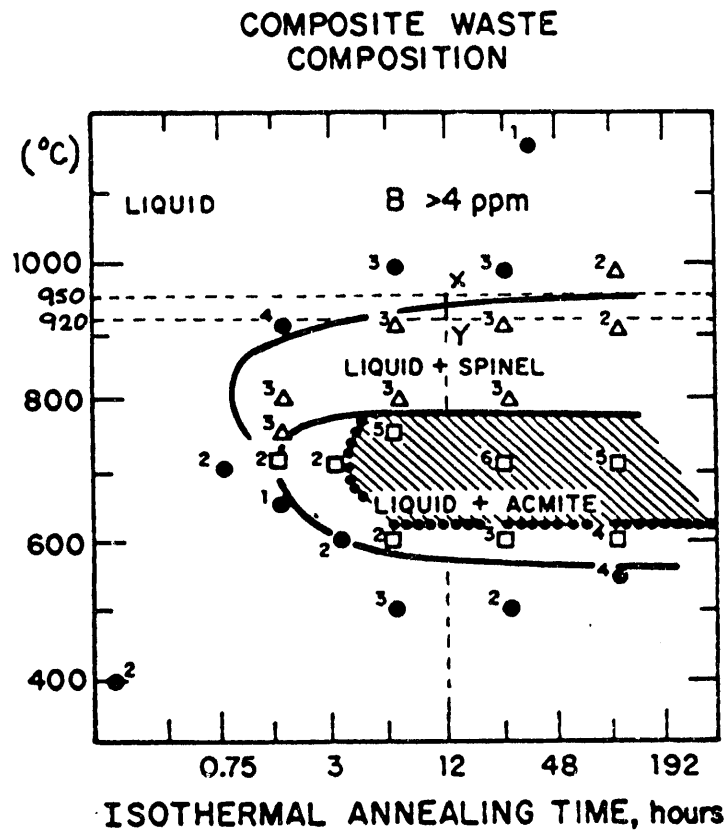
**COMPOSITE WASTE
COMPOSITION**

FIGURE 6. Time-Temperature-Transformation Diagram for
SRL-165 Composite Waste Glass, from Jantzen
and Bickford.[9]

Test II. Freeze and Restart Campaign

Freezing of the Melt Pool

After Test I was completed on 6/12/88, the melt pool was maintained at idle conditions with no feeding or pouring, until Test II began on 6/16/88. In order to allow the melt pool to cool, all of the SGM heating components were turned off, including both electrodes and the riser, pour spout, lid, and dump valve heaters, and this point was marked as time zero. Throughout Test II, the off-gas and melter shell cooling water systems remained on-line.

As shown in Figure 7, the melt temperatures measured in the East thermowell were initially between 1000°C and 1180°C and fell below 515°C within 24 hours. The vertical temperature gradient was the largest near the melt surface, and the maximum melt temperature was shifted to the lower regions of the pool with time. This indicates that the net heat loss at the surface by radiation and convection was more significant than the conductive heat loss below the melt line.

During the first 12 hours of cooldown, the average cooling rate of the bulk melt between $z = 1.5"$ and $20.75"$ was $41.5°C/hr$, where z is the melt depth. At the 12 hour mark, the maximum melt temperature of 715°C was measured at $z = 12.5"$ in the East thermowell, and this
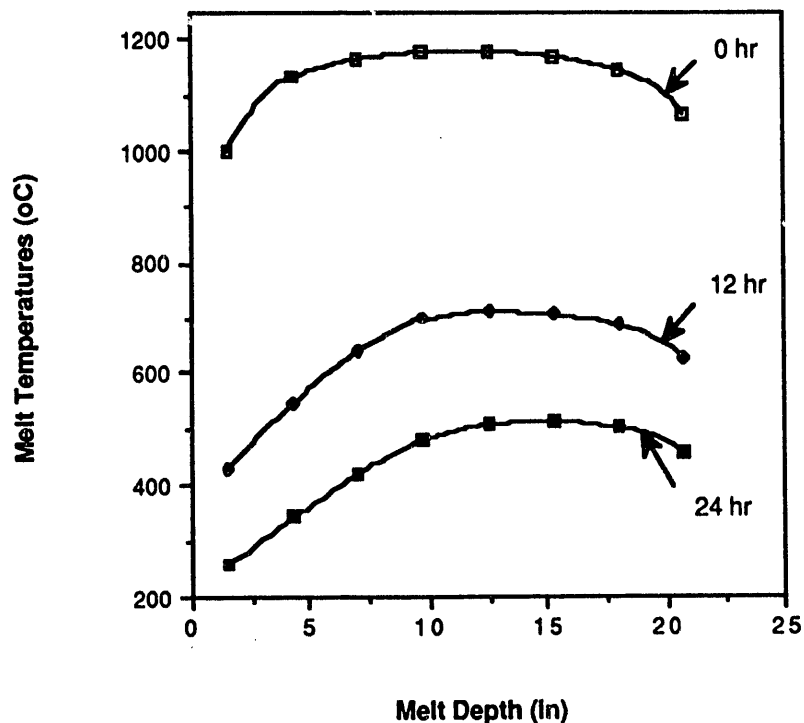
FIGURE 7. Vertical Melt Temperature Profiles during 24 Hour Cooldown in the East Thermowell.

is approximately the lowest temperature required for the initiation
of joule heating. During the next 12 hours, the average cooling
rate was decreased to 16.5°C/hr. At the 24 hour mark, the maximum
melt temperature was ~515°C, and it was measured at z = 15.25".

The total air flow rate in the plenum space was maintained fairly
constant at 305-320 pph. The backup off-gas film cooler (BUOGFC)
air flow and the total air purges for TV camera and seal pot were
kept at 120 and 40 pph, respectively, and the melter air inleakage
rate ranged from 145 to 160 pph.

Heatup with Upper Lid Heaters

About 26 hours after the melt pool began to cool, all the measured
melt temperatures fell below 500°C, which is close to the softening
point of glass. The melter was restarted at this point by heating
the frozen glass using only the upper lid heaters whose surface was
initially at ~100°C. The purpose of this setup was to simulate the
restart of the DWPF Melter with both sets of the lower dome heaters
inoperable. The convective heat loss was minimized by turning off
the BUOGFC air flow and by increasing the melter pressure from -5"
to -1.1" wc.

Initially, amperage was manually ramped to the lid heaters, until
the lid heater surface temperature monitored by the Low Temperature
Monitoring System (LTMS) reached 350°C. At these low temperatures,
the rate of lid heater surface temperature rise was recommended to
be less than 10°C/hr, and the actual rate of rise averaged 22°C/hr.
Since the Distributed Control System (DCS) is capable of accurately
reading the thermoelectric signals on a microvolt scale, the LTMS
is not necessary during the DWPF Melter startup. At temperatures
above 350°C, the automatic temperature controller (310 TC) was used
to uniformly increase the surface temperature at a rate of 20°C/hr
to the short-term operating limit of 1050°C. The hot spots on the
lid heaters are located at the end of the lid heater tubes opposite
to the power supply connections, and the hot spot temperatures were
maintained below 1100°C at all times.

The melt temperatures at three different vertical positions in the
East thermowell are next plotted in Figure 8 as a function of time
during the entire Freeze/Restart campaign. As expected, the melt
temperatures continued to decrease for some time after the radiant
heating was initiated. Due to its close proximity to the surface,
the melt at z = 1.5" was the first to rise 15 hours after the upper
lid heaters were energized. During this 15 hour induction period,
the melt temperature at z = 1.5" fell by 40°C, and this additional
temperature drop was increased with an increasing melt depth. The
temperature at z = 7.0" fell by 140°C before it began to rise 28
hours later. At z = 20.75", the additional temperature drop was
the largest at 220°C during the 56 hour induction period. At about
55 hour mark, all the measured temperatures were nearly identical,
indicating zero conduction in the vertical direction.
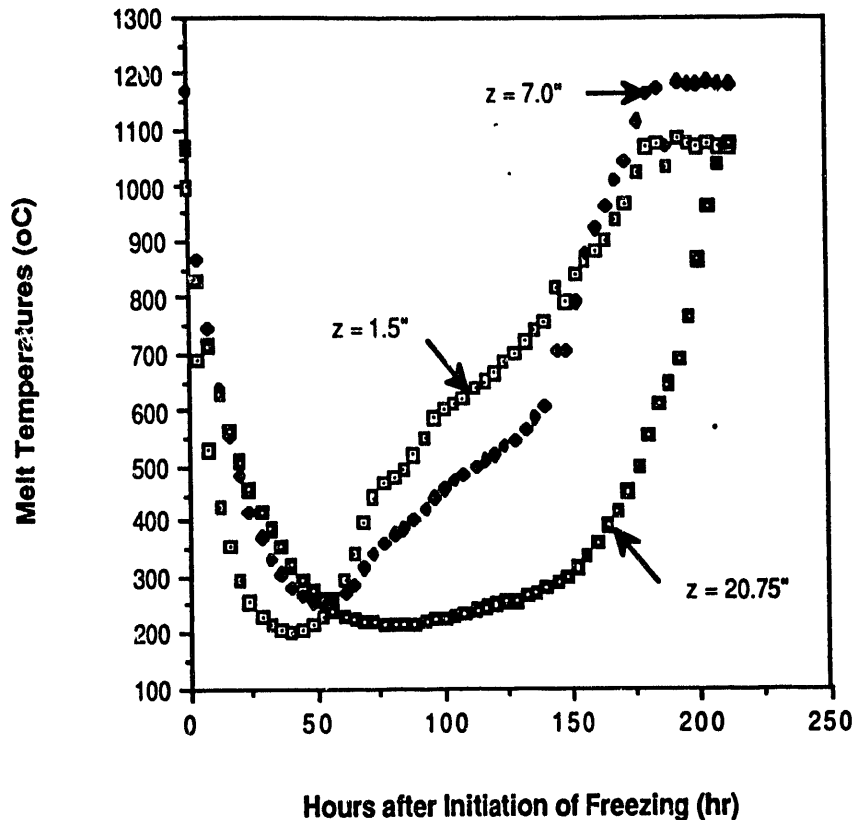
FIGURE 8. **Variation of Melt Temperatures in the East Thermowell during the Entire Campaign Cycle.**

The vertical profiles of melt temperatures are plotted in Figure 9 at several different time marks of operational significance during Test II. After falling by more than 750°C during 26 hour cooldown, the melt temperature at $z = 1.5"$ changed less than 30°C during the next 30 hours. This indicates that for the bulk glass matrix near the surface, the sum of net radiative heat flux and conductive heat flux from the lower regions of the pool was roughly being balanced by the convective heat loss at the melt surface.

At the 55 hour mark, the vertical temperature gradient is shown to be nearly zero, and the upper lid heater surface temperature was reaching near 700°C. From this point on, the melt temperatures in the upper regions began to increase considerably faster than in the lower regions, as the thermal radiation becomes the dominant mode of heat transfer at T > ~700°C. It was also at this point when the direction of heat conduction within the glass matrix was reversed from upward to downward. During the next 100 hours or so, the vertical temperature profile remained nearly a straight line with its slope steadily increasing with time except near the melter floor. At the 152 hour mark, the maximum melt temperature began to shift from the melt surface to the inner regions for the first time since the 55 hour mark.
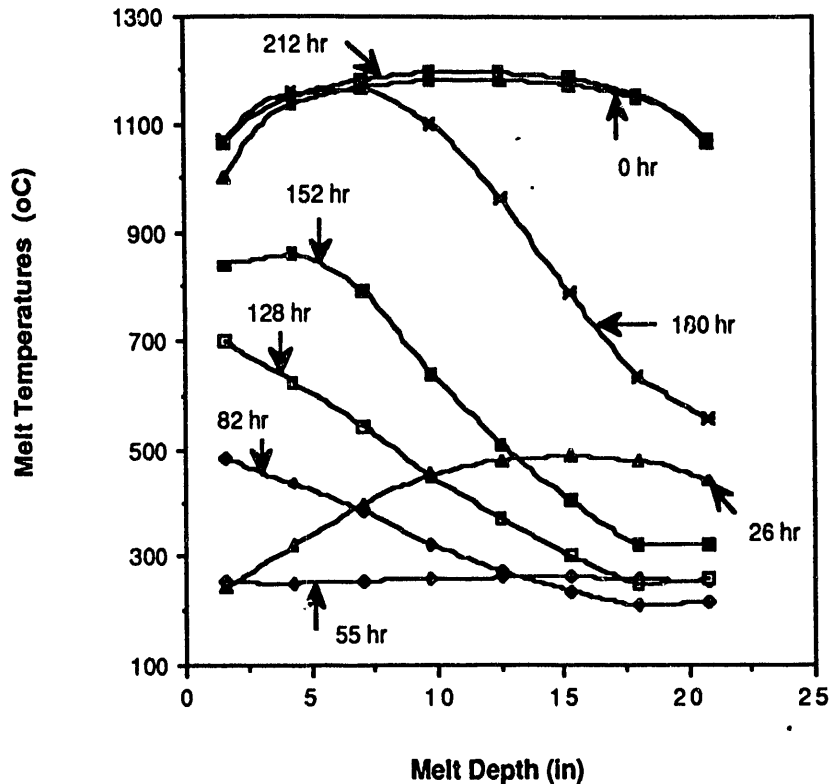
FIGURE 9. Variation of Vertical Temperature
Profile in the East Thermowell.

At the 65 and 67 hour marks, two five-minute power outages to the upper lid heaters were taken to increase the secondary lid heater current limit from 5480 to about 6200 amps. The maximum secondary amperage available was 6600 amps. No melt temperatures were found to be affected by these outages, but the vapor space temperature showed a decrease of ~20°C during each power outage.

The hot spot on the upper lid heaters reached its operating limit of 1100°C at the 70 hour mark. Under these limiting conditions, the upper lid heaters supplied 80 KW total or 6.8 KW/ft^2 of melt surface area for the next 12 hours (see Figure 10). The average rate of upper glass temperature rise was near 10°C/hr up to the 70 hour mark, but it was rising at only 2°C/hr near the 82 hour mark. At that point, the glass temperature at z = 1.5" was approaching only 490°C, and it was apparent that at this rate, the upper glass temperatures could not be raised above 700°C within a reasonable amount of time.

It was further noted that the upper lid heater surface temperature remained constant at 945°C during this 12 hour period, indicating that the short-term operating limit of 1050°C was unattainable even with the maximum power supply. As a result, the lower lid heaters were energized at the 82 hour mark, and its surface temperature was already reaching near 560°C at the onset of firing.
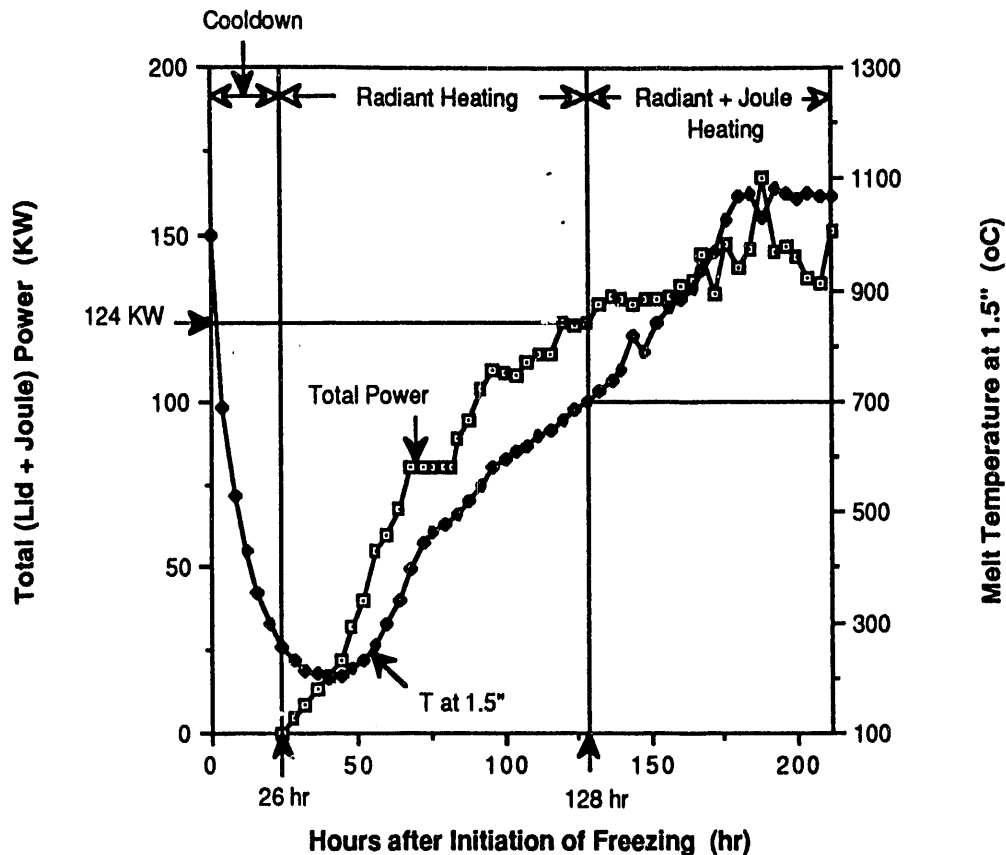
FIGURE 10. Effects of Lid and Joule Heating on Upper Melt Temperature at z = 1.5".

Startup of Lower Lid Heaters

In order to simulate the restart of the DWPF Melter with one of two lower dome heater sets inoperable, the lower lid heater power was slowly ramped to 40 KW or 1/2 of the maximum operating power at the 94 hour mark and maintained at that value during the next 12 hours. The hot spot temperature of the upper lid heaters was kept at near 1100°C throughout, and the lid heater power averaged 69 and 39 KW for the upper and lower ones, respectively, during the same period. The decrease in upper lid heater power from 80 to 69 KW despite the same hot spot temperature was due to a radiative heat contribution by the lower lid heaters on the hot spot of the upper lid heaters. This indicates that the hot spot temperature becomes the limiting factor for power supply during radiant heating.

During the same 12 hour period, the melt temperature at z = 1.5" rose from 584 to 613°C and was rising at only 2°C/hr near the end. It was apparent that the upper melt temperatures would not reach the 700°C mark, unless the lid heater power was further increased. Consequently, the lower lid heater power was increased by about 1 KW/hr during the next 22 hours. The melt temperature at z = 1.5" reached 695°C at the 128 hour mark, and the upper electrodes (C/D) were energized successfully.

At the onset of joule heating, the upper and lower lid heaters were supplying 62 KW each for 124 KW total (Figure 10) or 10.5 KW/ft² of melt surface area, and this is the total lid heater power typically required during slurry-feeding. It is noted that all the reported lid heater power readings did not include the radiative heat loss of ~11 KW around the lid heater cover box estimated earlier.[3]

Joule Heating via Upper Electrodes

Initially, the primary side of the electrode power transformer was configured on tap #3 with the secondary in series to provide 960 A at 300 V. During the first 17 hours of joule heating, a jumper was installed around the upper electrode isolation switch to accurately measure low amperages of up to 250 A using the clamp-on ammeters. The upper electrode power was slowly ramped at 2 KW/hr during the same period, and the melt temperature at z = 1.5" rose at ~8°C/hr.

At the 130 hour mark, the surface temperatures of both lid heaters reached well above 950°C, and the riser and pour spout heaters were energized. At the onset of firing, the hot spot temperatures on the riser and the pour spout were 170°C and 60°C, respectively, and the lowest melt temperature measured at that time was 250°C at z = 18" in the East thermowell. The power supply to these heaters was to be controlled in such a way that the hot spot on the riser was at least 10°C cooler than anywhere in the melt pool at all times. Similarly, the setpoint of the zone 1 dump valve heater was also to be controlled so that the heater temperature would not exceed the bulk melt temperature in the vicinity.

At the 145 hour mark, the upper electrode power was cut off for 35 minutes to remove the jumper and, as expected, the upper melt pool at z ≤ ~11" showed some moderate degree of temperature drop. For example, the melt temperature at z = 1.5" fell from 827°C to 787°C before it began to rise again 3 hours later at 8°C/hr. The heatup rate of the K-3™ refractory is limited to 10°C/hr to minimize the thermal stress in the brick and, consequently, the heatup rate of glass should always be less than 10°C/hr. It is noted that no such power outage to the electrodes will be necessary in the DWPF, since no jumper will be used.

Near the 169 hour mark, the average melt temperature in the upper regions was reaching 950°C, and the estimated glass resistivity was ~7.9 Ω-cm, which is nearly one-sixth of that at 700°C. In order to supply more amperage, the upper electrode power was turned off for ~10 minutes to reconfigure the primary side of the upper electrode power transfomer to tap #2 with the secondary in parallel position. The upper electrodes were then capable of providing the melt with 2742 A at 105 V. Figure 11 shows that the upper melt temperatures were decreased by ~25°C due to this 10 minute power outage before they all began to rise again about 30 minutes later. However, the lower melt termperatures at z ≥ 12.5" remained relatively constant or kept increasing during the same period. This short power outage will be required also in the DWPF.

```
C-D ELECTR AMPS      GLASS TH/WALL 18     GLASS TH/WALL 07     GLASS TH/WALL 17
   358     AMPS        229      DEG C       217      DEG C       228      DEG C
W------------------W  X------------------X Y------------------Y Z------------------Z
      1000.00              1050.00              1050.00      z = 7"   1050.00
   X         X                                                   ↓
                                         X        X  990.00      X        X
      800.00              990.00                                          990.00
                                                              z = 9.75"
                                                                 ↓
   Z  600.00  Z        Z  930.00  Z               930.00       Z       930.00
   W         W                         Z                                        Z
                                                                  ↓
      400.00   C/D Amps  870.00            W   870.00    W         870.00
                                     W
                                                              z = 12.5"
      200.00              810.00              810.00             810.00
                                                                 ↓
   Y         Y         Y              Y                      Y              Y
 1000    0.00   1022   W 750.00   1045    750.00    1107     750.00    1130
23-JUN-88
```
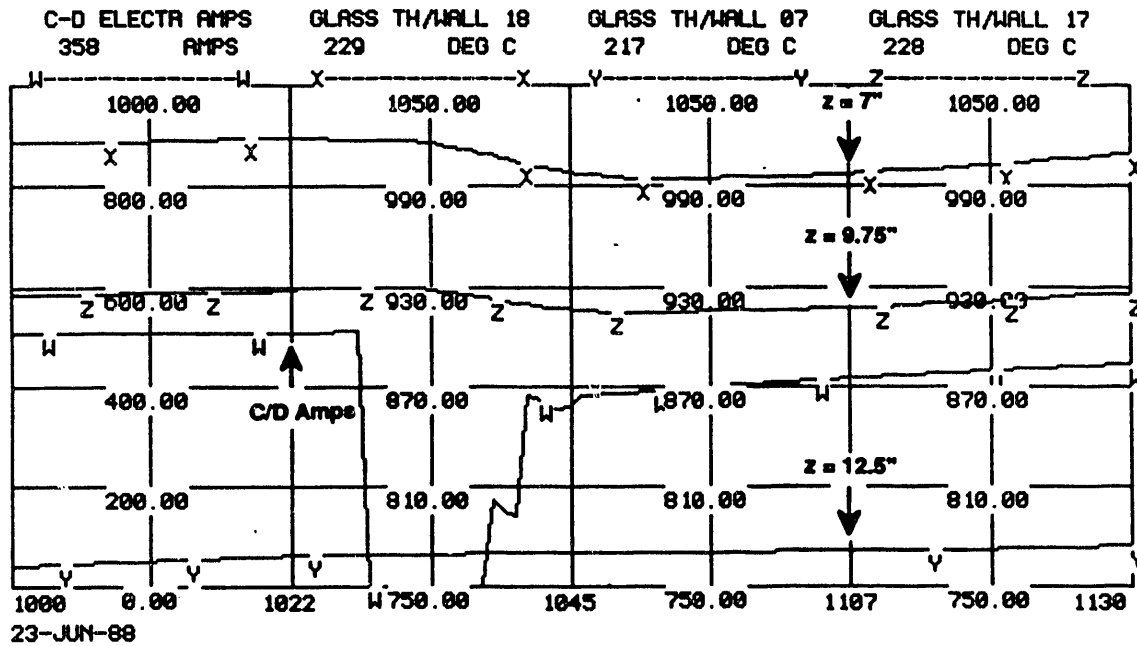
FIGURE 11. Effect of Power Outage on Melt Temperatures during Transfomer Tap Change.

Joule Heating via Lower Electrodes

At the onset of firing at the 180 hour mark, the melt temperatures along the 8" height of the lower electrodes (A/B) ranged from 520°C near the bottom to 850°C near the top, and the midpoint temperature was estimated to be 635°C. By comparison, when the upper electrodes were energized at the 128 hour mark, the melt temperatures ranged from 525°C near the bottom to 710°C near the top of the 7.5" high submerged portion, but the midpoint temperature was also estimated to be ~635°C. During an earlier startup attempt with fresh frit,[7] the melt temperature at the midpoint of the lower electrode height was also ~635°C at the onset of joule heating.

In all cases mentioned above, the thermocouples were positioned at an equal radial distance of 4.5" away from the wall, and the front face of electrodes was also at a comparable distance away from the wall, from ~1.2" at the sides to ~5.25" at the center. Therefore, noting the large temperature variations along the electrode height, the melt temperatures between 630 and 640°C at the midpoint of the front face of electrodes appears to be a good criterion for when to attempt joule heating.

At the 186 hour mark, both upper and lower electrode power was cut off for 45 minutes to remove the jumper from the lower electrodes and to change the lower electrode power transformer setting from the series (tap #3) to the parallel position (tap #3) in order to provide 1920 A at 150 V. At the time of power outage, the lower electrodes were supplying ~20 KW, while close to 90 KW was being supplied by the upper ones. As a result of power outage, the upper melt temperatures fell more than 100°C during the next hour, while the temperature drop in the lower region was less than 40°C.

With joule heat continuously supplied, the lower melt temperatures began to rise considerably faster from the 180 hour mark, as shown in Figure 9, while the maximum melt temperatures remained virtually unchanged. At the 212 hour mark, the vertical temperature profile returned nearly to its steady state form, and both lid heaters were deenergized to prepare for the final pouring and draining.

Thermal Symmetry

The melt temperatures were measured at two different positions in the radial direction, i.e. East and West thermowells. Furthermore, both the lid heaters and the electrodes were configured in such a way that both thermowells were equally influenced by each of these heaters. Therefore, the radial comparison of melt temperatures at comparable melt depths may identify any design and/or operating parameters which can distort the thermal symmetry of the melt pool. In order to examine how well this thermal symmetry was preserved during the course of freeze and restart, the melt temperatures were radially compared in Figure 12 at three different melt depths, and some degree of thermal asymmetry seems apparent during the heatup period, especially in the upper region. To demonstrate this better visually, the absolute temperature differences between the East and West thermowells are plotted in Figure 13, and they are shown to be as large as 110°C.

The differences between the two melt temperature measurements made side-by-side at each depth in the West thermowell are next plotted in Figure 14. It shows that the melt temperatures fluctuated less than ±10°C initially as well as during cooldown at all depths, and some moderate fluctuations are expected even during steady state operations due to a highly viscous and relatively non-conductive nature of melt as well as the inherent fluctuations in thermocouple response. As portions of the melt pool were heated or still being cooled at varying rates during later hours, this increased thermal inhomogeneity is seen to induce fluctuations as large as 50°C, and the fluctuations became less intensified toward the end of Test II.

Consequently, the temperature fluctuation of 50°C can be considered as the maximum thermal instability inherently characteristic of the melt at every spatial point within the pool. Furthermore, as shown in Figure 13, whenever the East and West temperature difference is within ±50°C, it may then be said that the overall thermal symmetry was maintained at that time.
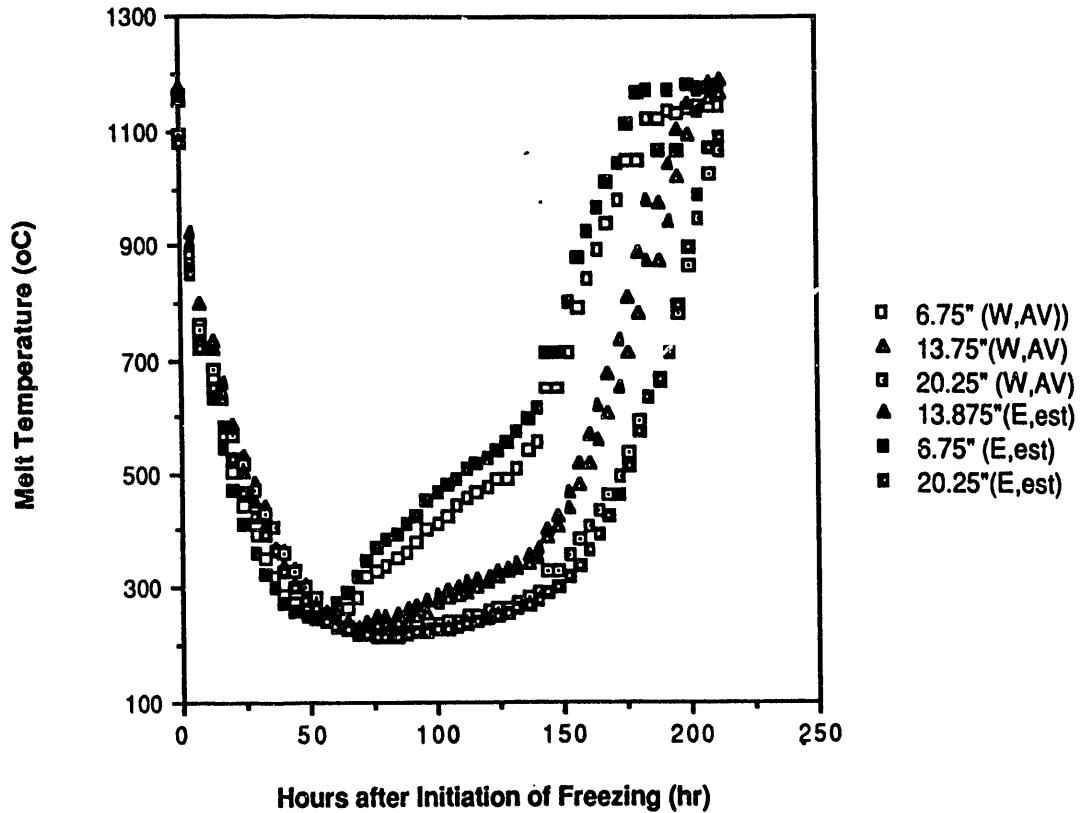
FIGURE 12. Comparision of Melt Temperatures
in the East and West Thermowells

Figure 13 shows that all the East and West temperature differences were within ±25°C initially, indicating the thermal symmetry of the melt pool during idling. It is also noted that the profile of East and West temperature differences at each depth exhibited a similar overall pattern in time. During cooldown, the melt temperatures in the East thermowell fell at slightly higher rates than those in the West thermowell at all depths, as indicated by the negative slopes. When the restart was initiated at the 26 hour mark, this trend was reversed, and the profiles began to separate out from one another near the 50 hour mark, as the temperature fluctuation profiles did in Figure 14. During all these periods, the absolute East and West temperature differences were still within the expected fluctuation at all depths, thus maintaining the overall thermal symmetry. This also indicates that the riser channel has no significant effect on the thermal characteristics of the bulk melt, maybe except in its immediate vicinity.

Figure 13 also shows that the East and West temperature difference at z = 6.75" began to increase beyond the expected fluctuation near the 130 hour mark and reached its maximum of 90°C at about 155 hour mark. At the 152 hour mark, the maximum melt temperature was found earlier in Figure 9 to have shifted from the melt surface to about 5" below. This deviation from a linear vertical temperature profile was clearly induced by continuous supply of joule heat in the upper
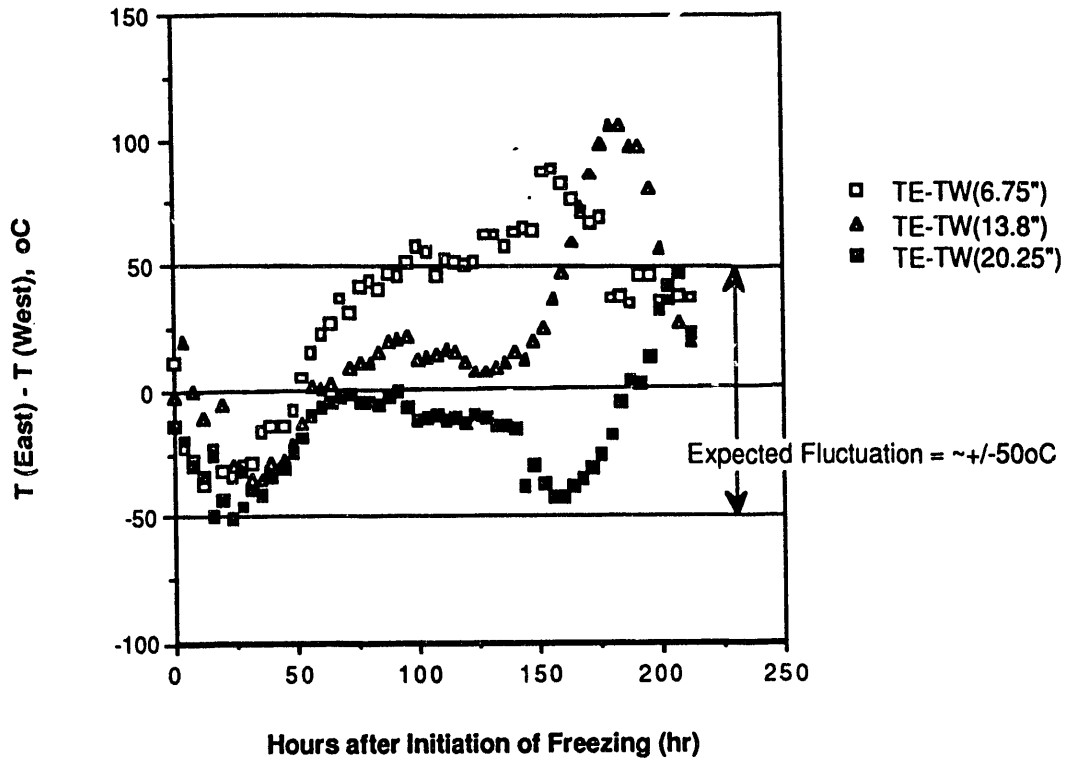
FIGURE 13. Temperature Differences between East and West Thermowells during Freeze and Restart
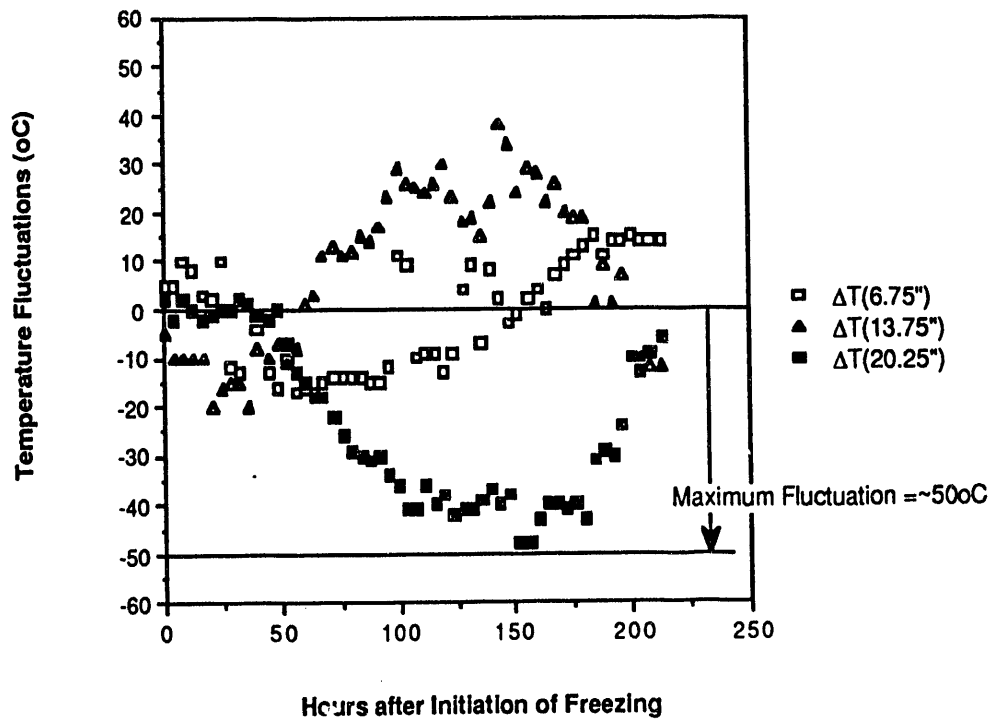

FIGURE 14. Fluctuations in Temperature Measurements

regions since the 128 hour mark, which in turn may have established
significant convective flows at that thermocouple location near the
155 hour mark. This hypothesis appears to be consistent with the
PNL simulation results shown in Figure A.1 in Appendix. Similarly,
at z = 13.8" or near the top of the lower electrodes, the maximum
thermal asymmetry was at about 185 hour mark, 5 hours after joule
heating was established in the lower regions. Therefore, it seems
that the overall thermal symmetry is most likely to be disturbed at
the onset of significant convection and, once the convective flows
are fully developed, the melt pool retains its thermal symmetry.

The melt temperature at the point of maximum thermal asymmetry was
next estimated at the peak of each profile in Figure 13. They are
shown in Figure 15 to increase with increasing z, indicating that
it becomes more difficult to establish convective flows as the melt
depth increases. It is further noted that as the heatup rate began
to increase, the degree of thermal asymmetry was also increased and
reached its maximum at the highest heatup rate, as shown in Figure
16 for z = 6.75".

More pronounced thermal asymmetry was also observed earlier during
a startup with fresh frit.[7] After joule heating was established,
the East and West temperature differences of up to 300°C were seen,
but they all fell within the expected range of fluctuation later at
temperatures above 1000°C.[7] The formation of these so-called hot
and cold spots was attributed to a non-uniform distribution of the
electrode current through the frit matrix which was being melted
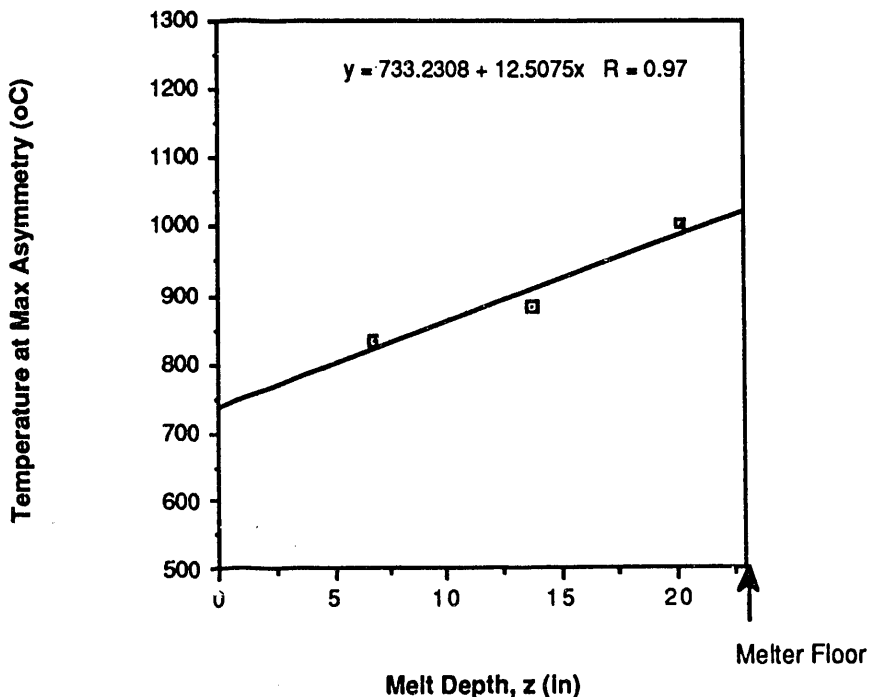for the first time and thus contained a great deal of void space.

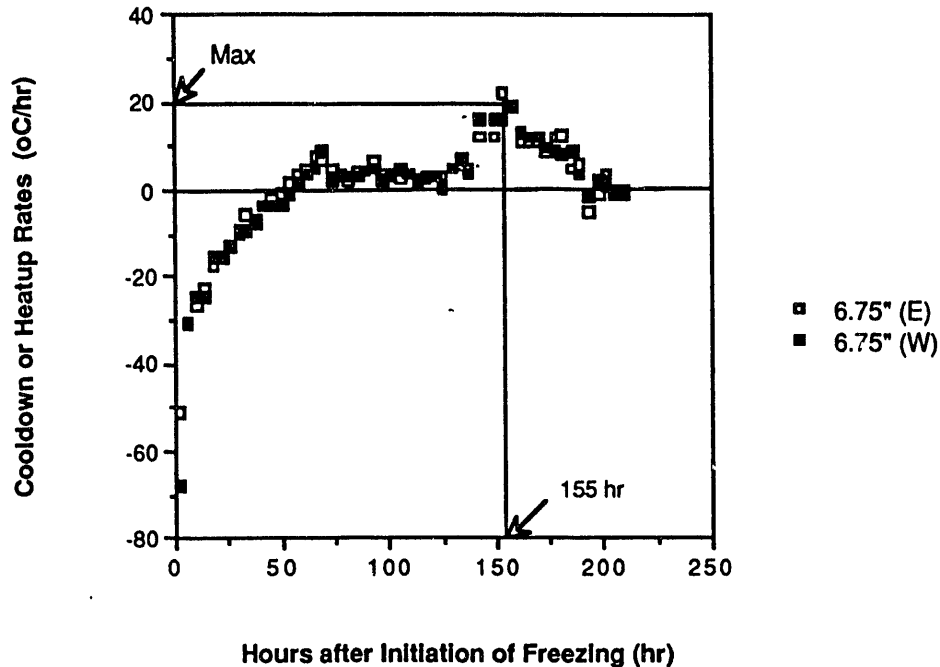FIGURE 15. Melt temperatures at Maximum Thermal Asymmetry

FIGURE 16. Comparison of Cooldown and Heatup Rates in the East and West Thermowells at z = 6.75".

COMPARISON OF MELTER STARTUP CAPABILITIES

It was mentioned earlier that the startup capability of the DWPF Melter was expected to be greater than that of the SGM,[2] based upon the ratio of nominal lid heater power to melt surface area in each melter. However, during the radiant heating period, it is the net radiant heat flux incident on the glass surface that determines the actual rate of rise in glass temperatures, rather than the nominal lid heater power flux itself. The net incident radiation should be calculated by considering every radiative heat exchange among all surfaces involved. Furthermore, it is important to make sure that the relative startup capabilities of any two melters are compared under the identical operating conditions such as the same rate of lid heater surface temperature rise. Hence, there is a need for a plenum radiative heat transfer model even in this comparison study, and one such simple analysis is described next.

Radiative Heat Transfer in the Plenum

Here the plenum is envisioned as a cavity enclosed by 3 surfaces; (1) glass surface, (2) lid heater tube surfaces, and (3) refractory walls and lid. It is assumed that all surfaces are diffuse, while all bodies are grey. The net radiative heat flux incident on the glass surface is then given by

$$H_1 - J_1 = \delta_1 \, \rho_1 \, C_{p1} \, (dT_1/dt) \tag{2}$$

where H is the incident radiation flux, J is the radiosity, ρ is the density, C_p is the mean specific heat capacity, δ is the effective thickness of a surface of interest, and the subscript 1 refers to the glass surface.

For most solids, all of the incident radiation is absorbed in a very thin layer of thickness δ below the surface, and the solution to Eq.2 then becomes the transient temperature boundary condition for the differential energy balance equation of the entire glass matrix. However, during most of the radiant heating period, the glass temperatures near the melter floor were seen in Figure 9 to vary by less than 50°C between 55 and 128 hour mark. Much larger temperature variations were observed during the initial stages of radiant heating between 26 and 55 hour mark, but this was because the glass matrix in the lower regions lost the conductive heat not only through the refractory walls but also to the glass matrix in the upper regions which was at lower temperatures.

Therefore, if the entire glass matrix were initially at a uniform temperature, the net conductive heat flux through the lower glass matrix can be assumed to be equal to the conductive loss through the refractory, thus maintaining relatively constant temperatures. This assumption greatly simplifies the calculational tasks, since Eq.2 itself now describes the transient thermal characteristics of the bulk glass close to the surface without having to solve another energy balance equation for the entire glass matrix simultaneously.

It is further assumed in Eq.2 that there is no radial variation in glass temperatures and that the convective heat flux at the surface is equal to the conductive flux to the lower region. The latter is a rather drastic but still acceptable assumption for just comparing the relative startup capabilities, since its effects on upper glass temperatures are likely to be comparable in both melters. Moreover, the validity of this assumption will increase, as radiation becomes increasingly dominant with increasing temperature.

Using the reciprocity theorem, the incident radiation on the glass surface is given by

$$H_1 = N \, F_{12} \, J_2 + F_{13} \, J_3 \tag{3}$$

where N is the total number of lid heater tubes, and F_{ij} is the view factor from surface i to surface j.

The radiosity from surface i is further defined as

$$J_i = \tau_i \, H_i + \varepsilon_i \, E_{bi} \tag{4}$$

where τ and ε are the reflectance and the emittance, respectively, and E_b is the intensity of the black body radiation at T_i.

Combining Eqs.2-4 and after some algebraic manipulations, the net radiative heat flux at the glass surface becomes

$$\delta_1 \; \rho_1 \; C_{p1} \; (dT_1/dt) = (\beta_1 F_{21} - 1) \; \varepsilon_1 \; \sigma \; T_1^4 + (\beta_1 \varepsilon_2 \; /(1 - \varepsilon_2)) \; \sigma T_2^4$$

$$+ \; (\beta_1 \; F_{23} + F_{13}) \; \varepsilon_3 \; \sigma \; T_3^4 \qquad\qquad (5)$$

where $\beta_1 = N \; F_{12} \; (1 - \varepsilon_2)/(1 - (1 - \varepsilon_2) \; n \; F_{22})$, and n is the number of neighboring lid heater tubes to which each lid heater tube can emit radiation, and σ is the Stefan-Boltzmann constant, 56.7×10^{-12} kW/m^2.K^4. It is further assumed that $\varepsilon_1 = \varepsilon_3 = 1.0$, and $\varepsilon_2 = 0.8$.

By the same analogy, the net radiative heat flux at the refractory walls and the lid is given as

$$\delta_3 \; \rho_3 \; C_{p3} \; (dT_3/dt) = (\beta_3 \; F_{21} - F_{31}) \; \varepsilon_1 \; \sigma \; T_1^4 + (\beta_3 \; \varepsilon_2/(1 - \varepsilon_2)) \; \sigma \; T_2^4$$

$$+ \; (\beta_3 \; F_{23} + F_{33} - 1) \; \varepsilon_3 \; \sigma \; T_3^4 \qquad\qquad (6)$$

where $\beta_3 = N \; F_{32} \; (1 - \varepsilon_2)/(1 - (1 - \varepsilon_2) \; n \; F_{22})$. It is important to note that in Eq.6, the convective heat flux at the refractory walls and the lid was assumed to equal the conductive heat flux through the refractory. This becomes a valid assumption, when the melter is operated at high temperatures under steady state conditions, as in typical industrial furnaces.

Estimation of Parameters

The lid heater surface temperature, T_2, which is the only operating variable to be considered, was increased linearly up to the normal operating limit of 950°C and maintained at that value thereafter. Most of the parameters included in Eqs.5 and 6 are concerned with the plenum geometry and the arrangement of the lid heater tubes. The view factors estimated for the 3-component model are summarized in Table A.3. Also included in the table are the view factors for the 4-component model in which the plenum is assumed to be enclosed by 4 surface elements; (1) glass, (2) lid heater tubes, (3) melter lid, and (4) refractory walls. The value of n is different for the inner and outer lid heater tubes for the DWPF Melter and has the average value of 5.5, while it is constant at 3 in the SGM.

Initially, all surfaces were assumed to be at a uniform temperature
of 500 K, and no temperature gradient was assumed to exist within
the glass pool. The thermal characteristics of the bulk glass near
the surface should then be insensitive to the melter geometry below
the melt line throughout the radiant heating period. Consequently,
the effective thickness of the glass surface, δ_1, can be assumed to
be identical for the two melters. At the onset of joule heating,
the glass temperature at z = 1.5" was ~700°C, and this was close to
the average glass temperature between z = ~0 and z = 4.25" where
the second thermocouple from the melt line was located. Therefore,
δ_1 was assumed to be 4.25" in the simulation, and joule heating was
allowed to be self-sustained, when T_1 reached 700°C.

The effective thickness of the refractory walls and lid, δ_3, is an
adjustable parameter and difficult to estimate due to lack of the
thermal data within the refractory. Therefore, several different
δ_3's were assumed to see its effect on T_1. All physical properties
were assumed to be constant and evaluated as the average between
200 and 800°C. Table A.4 further summarizes the estimated values
for the parameters used in the simulation. Eqs.5 and 6 were solved
simultaneously using the fourth-order Runge-Kutta computer program
written by L. Lee of SRL.

Results and Discussion

In case A, the surface temperature of the lid heaters was increased
at 10°C/hr, and its actual rate of rise during the radiant heating
period of Test II averaged ~9°C/hr. Noting that glass has a much
higher transmittance than other types of electrically nonconducting
materials, the effective thickness of the refractory was assumed to
be 0.425" in the SGM, exactly 1/10 of that of the glass matrix.

In the DWPF Melter, the effective refractory thickness was assumed
to be 0.34", smaller than that in the SGM by a factor of 0.8 which
is the ratio of average refractory thickness of the SGM plenum to
that of the DWPF Melter plenum (~8.5"/~10.5"). Obviously, this was
to account for a lower conductive heat loss per unit area of plenum
in the DWPF Melter. Figure 17 shows that both melters exhibited a
virtually identical thermal behavior, and joule heating was started
in just 48 hours after the radiant heating began. The largest
glass temperature difference observed during heatup was only 10°C.

In case B, the effective refractory thickness of the SGM plenum was
assumed to be 4.13", and this is equal to 1/2 of the average plenum
refractory thickness. With δ_3 chosen comparable to the refractory
dimension, the wall temperatures will be lower than in case A, and
the purpose was to implicitly simulate larger conductive heat flux
through the refractory than in case A. The value of δ_3 assumed for
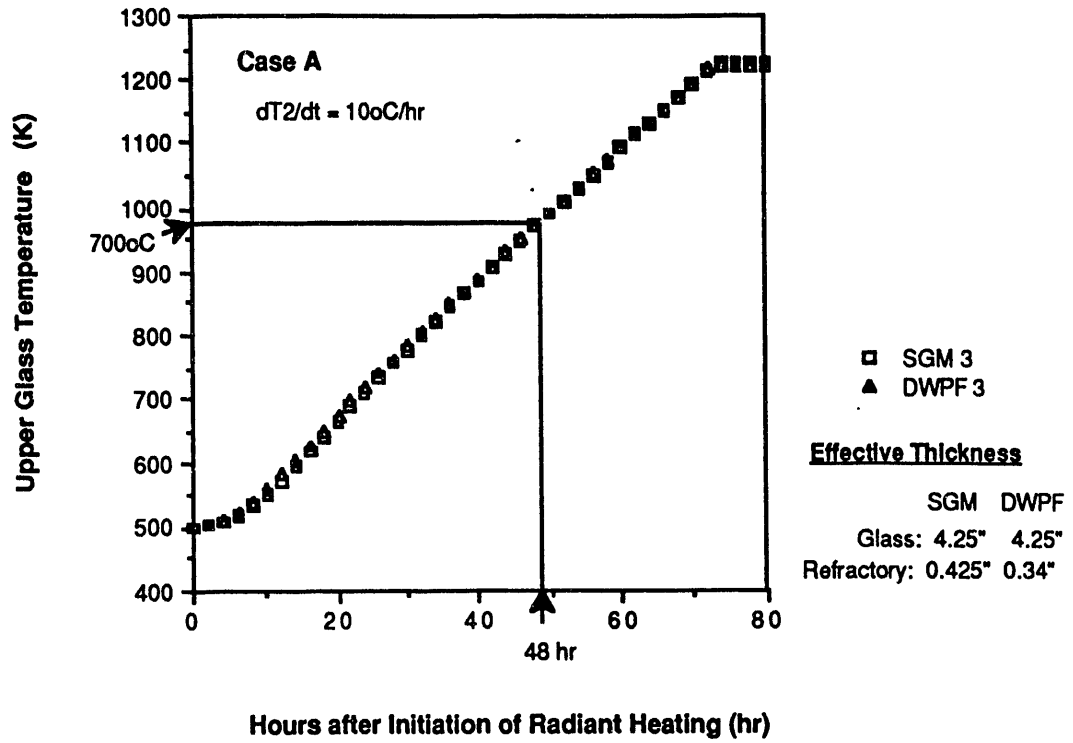the DWPF Melter was 3.31", again smaller by a factor of 0.8.

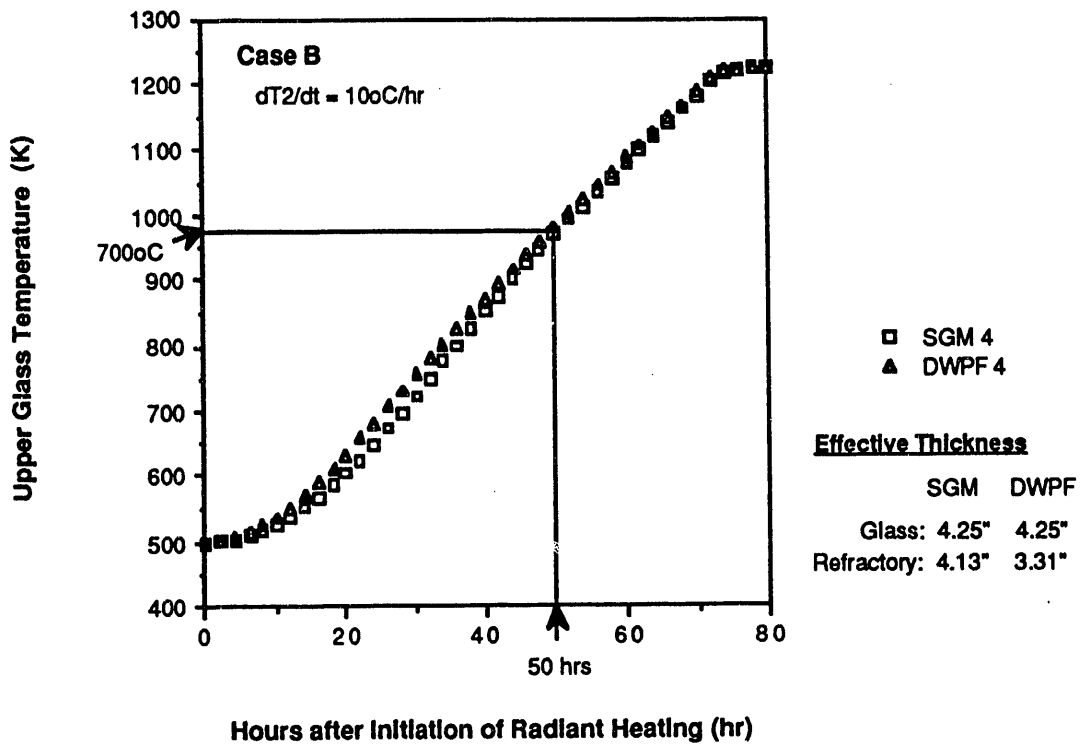**FIGURE 17.** Transient Upper Glass Temperatures in Case A

FIGURE 18. Transient Upper Glass Temperatures in Case B

At the same rate of lid heater surface temperature rise as in case A, Figure 18 shows that the initiation of joule heating in case B is a little easier in the DWPF Melter than in the SGM but only by an hour. The overall thermal characteristics of both melters still remain quite indistinguishable, and the glass temperatures in the DWPF Melter are at most 35°C higher than those in the SGM.

Although not shown here, it is also noted that when the rate of lid heater surface temperature rise was doubled to 20°C/hr, the glass temperatures in the two melters reached the 700°C mark again within the same time of ~27 hours. If the effects of joule heating were included in the present analysis, the glass temperatures would be increased more rapidly at $T_1 \geq$ ~700°C, rather than asymptotically approaching a limiting value of 950°C or 1223 K.

Figures 17 and 18 also show that the radiant heating time required to initiate joule heating is quite insensitive to the effective refractory thickness. In the SGM, with δ_3 nearly 10 times as large in case B, it took only ~2 hours longer to initiate joule heating than in case A. This indicates that the assumption of considering the refractory walls as reradiators may be reasonably valid also in our transient analysis. The effective glass thickness also showed little effects on the transient thermal behavior of glass perhaps due to its low thermal conductivity.

In Table 1, the net radiative heat flux at the glass surface is further broken down into the contribution from each surface at the onset of joule heating. Regardless of the effective refractory thickness considered, ~75% of the total incident radiation in the SGM is seen to come from the refractory walls and the lid, while only ~25% of the total incident radiation comes directly from the lid heaters. This is why the ratio of nominal lid heater power to melt surface area is not an accurate measure of the melter startup capability. In the DWPF Melter, on the other hand, nearly 35% of the total incident radiation comes directly from the dome heaters, and the remainder arrives after many reflections at the walls and the lid.

Although not shown here, it is further noted that the relative or fractional contribution from each surface to the total incident radiation changed little during most of the radiant heating period in each melter. These results indicate that the distribution of the total radiative heat transfer among all surfaces involved is characteristic of plenum geometry and lid heater configuration, and it is quite insensitive to the conductive heat transfer through the refractory walls.

The total lid heater surface area in the DWPF Melter is ~2.7 times larger than that in the SGM and, as expected, Table 1 shows that the incident flux from the lid heaters is ~1.5 times larger in the DWPF Melter than in the SGM. However, this difference is shown to be compensated for by the corresponding difference in the incident flux from the walls and lid, resulting in a constant incident flux

TABLE 1. Components of Radiative Heat Flux into Glass
at the Onset of Joule Heating, T_1 = 700°C.

Case	Melter	Net Flux (W/ft^2)	Lid Heaters (KW/ft^2)	Walls & Lid (KW/ft^2)	Glass (KW/ft^2)
A	SGM	90	1.13 (23%)	3.69 (77%)	-4.72 (98%)
A	DWPF	100	1.68 (35%)	3.14 (65%)	-4.72 (98%)
B	SGM	100	1.19 (25%)	3.63 (75%)	-4.72 (98%)
B	DWPF	100	1.74 (36%)	3.08 (64%)	-4.72 (98%)

of 4.82 KW/ft^2 of melt surface in each melter. Table 1 also shows
that regardless of the effective refractory thickness, nearly 98%
of the total incident radiation is emitted back into the plenum
from the glass surface at 700°C, thus resulting in a small net flux
ranging from 90 to 100 W/ft^2 of melt surface in both melters. The
net incident flux remained between 80 and 100 W/ft^2 of melt surface
during most of the radiant heating period, and this is reflected on
the relatively constant rate of rise in glass temperatures between
10 and 13°C/hr in Figures 17 and 18.

In summary, there seems to be little difference between the startup
capabilities of the two melters. This conclusion is solely based
on the assumptions made in the analysis, although they are thought
to be appropriate for the comparison purposes. The conductive heat
flux both above and below the melt line was estimated earlier to be
~1.25 times smaller in the DWPF Melter than in the SGM. However,
the total plenum surface area is nearly twice as large in the DWPF
Melter, which will make the total conductive heat loss in the DWPF
Melter ~1.5 times larger than in the SGM. This may be one reason
why the startup capabilities of the two melters are very similar
despite a greater lid heater power to melt surface area ratio in
the DWPF Melter.

CONCLUSIONS AND RECOMMENDATIONS

1. The startup temperature for joule heating of the DWPF startup glass is 25°C higher than that of the SGM Freeze/Restart glass.

2. In case of total power loss to the lower electrodes, the melt near the bottom reaches the DWPF operating limit of 200 poise in 12 hours. Spinel crystals will begin to form in the pool containing SRL 165 composite waste glass about 12 hours after the limiting viscosity range is reached.

3. The melt temperatures fell below the softening point of glass within 26 hours after all of the melter heating components were turned off. The average cooling rate was 28°C/hr.

4. The melt temperature drop measured during the induction period was as much as 220°C and increased with increasing melt depth.

5. During most of the 100 hour radiant heating period, the melt at $z \geq 15"$ showed temperature changes of less than 50°C, and the vertical temperature profile within the glass pool remained a straight line with an increasing slope in time.

6. During radiant heating, the hot spot temperature on the lid heaters becomes the limiting factor for power supply.

7. At the onset of joule heating, the total lid heater power flux was 10.5 KW/ft^2 of melt surface area, which is a typical value required during slurry-feeding.

8. The melt temperatures of 630-640°C at the geometric midpoint of the electrode front face appear to be a good criterion for when to attempt joule heating.

9. During 10-minute power outage to the upper electrodes for power transformer tap change, only the melt temperatures at $z \leq \sim 11"$ showed a decrease of ~25°C.

10. A maximum fluctuation of 50°C is inherently expected in every melt temperature measurement during freeze and restart.

11. The thermal symmetry of a melt pool is likely to be disturbed when significant convective flows are developing sometime after initiation of joule heating. The extent of these disturbances is more pronounced during a startup with fresh frit.

12. The riser channel has no effect on the thermal behavior of the bulk melt.

13. The startup capabilities of the SGM and DWPF Melter are quite similar under the identical operating conditions, despite the greater lid heater power per melt surface area in the latter.

14. During most of the radiant heating period, 25% of the radiative heat flux incident on the glass surface comes directly from the lid heaters in the SGM, whereas 35% of the total incident flux comes from the dome heaters in the DWPF. In each melter, the remainder is contributed by the refractory walls and lid in the plenum.

15. During most of the radiant heating period, nearly 98% of the radiation incident on the glass surface is emitted back into the plenum, resulting in a small net flux ranging from 80 to 100 W/ft^2 of melt surface in both melters.

ACKNOWLEDGEMENTS

QUALITY ASSURANCE

All Scale Glass Melter activities were performed in accordance with the Savannah River Quality Assurance Plan (DWP-82-111-2) and the Defense Waste Processing Section Quality Assurance Plan (DPST-QA-83-4-2). The QA plan assures that research, development, and demonstration are performed in a safe and controlled manner, so that the resulting technology data are valid and retrievable. The "Quality Assurance Review for Large Melter Test Facilities" (DPST-QA-86-2-1) describes in detail the QA Program for the Scale Melter Facility. All melter system instrumentation is calibrated on a QA schedule and is NBS traceable. All process run data is stored in the Vantage™ data collection system running on the Vax computer located in 679-T. The registered laboratory notebook that contains information related to this report is DPSTN-4464.

REFERENCES

1. Choi, I. G., "PNL's Final Report on SGM F/R Process Modeling," WSRC-RP-89-381, June 8, 1989.

2. Weisman, A. F., "Design Comparison of the Scale Melter to the DWPF Melter," DPST-87-688, October 7, 1987.

3. Yoshioka, M., "Energy Balance on the DWPF Scale Glass Melter, Runs 4-9," DPST-88-491, April 21, 1988.

4. Jantzen, C. M., Private Communication, February, 1989.

5. Plodinec, M. J., "Rheology of Melts Containing Crystalline Material," DPST-86-527, June 27, 1986.

6. Jantzen, C. M. and Plodinec, M. J., "Viscosity and Resistivity of Waste Glasses," DPST-86-372 Rev.1, May 15, 1989.

7. Baron, M. R. and Smith, M. E., "Summary of the Drain and Restart of the DWPF Scale Glass Melter," DPST-88-481, May 16, 1988.

8. Routt, K. R., "Glass Property Data for use in Design of the DWPF Melter," DPST-82-923, October 18, 1982.

9. Jantzen, C. M. and Bickford, D. F., "Leaching of Devitrified Glass Containing Simulated SRP Nuclear Waste, Mat. Res. Soc. Symp. Proc., 44, 135 (1985).

APPENDIX

TABLE A.1. **Comparison of Startup Frit Compositions.**

Components	Amount (wt%)		
	SGM Freeze & Restart	DWPF Startup	165 Black Frit
SiO_2	47.1	49.0	55.0
Fe_2O_3	13.4	13.5	11.3
Na_2O	12.8	11.5	11.0
B_2O_3	11.0	8.8	7.2
Al_2O_3	4.2	4.7	4.3
Li_2O	4.0	3.5	5.0
K_2O	0.8	2.6	-
MnO_2	2.1	2.3	2.5
CaO	1.4	1.2	1.4
NiO	1.2	1.1	0.9
TiO_2	0.3	1.0	-
MgO	0.6	0.7	0.7
Cr_2O_3	0.3	0.1	-
ZrO_2	0.5	-	0.7
SrO	0.3	-	-
Total	100.0	100.0	100.0

TABLE A.2. Constants for Fulcher-Tammann Equation
$\log_{10} \eta$ (poise) $= A + B/T(^\circ C)$.

Glass Type	A	B
SGM Freeze/Restart	-2.302	4349.109
DWPF Startup*	-2.247	4495.977
	-2.251	4466.020
	-2.247	4421.836
165-AV (DWPF Maximum)	-2.193	4574.629
131-AV (DWPF Minimum)	-2.152	4022.336

* The viscosity of the DWPF startup glass is estimated as the average of the three η's calculated.

SCALE GLASS MELTER: FLOW FIELD
CONV7A: VERTICAL CENTER PLANE – I = 2

PLOT FOR TYME =   547700.000

1.251

VERTICAL POSITION (M)

0.000

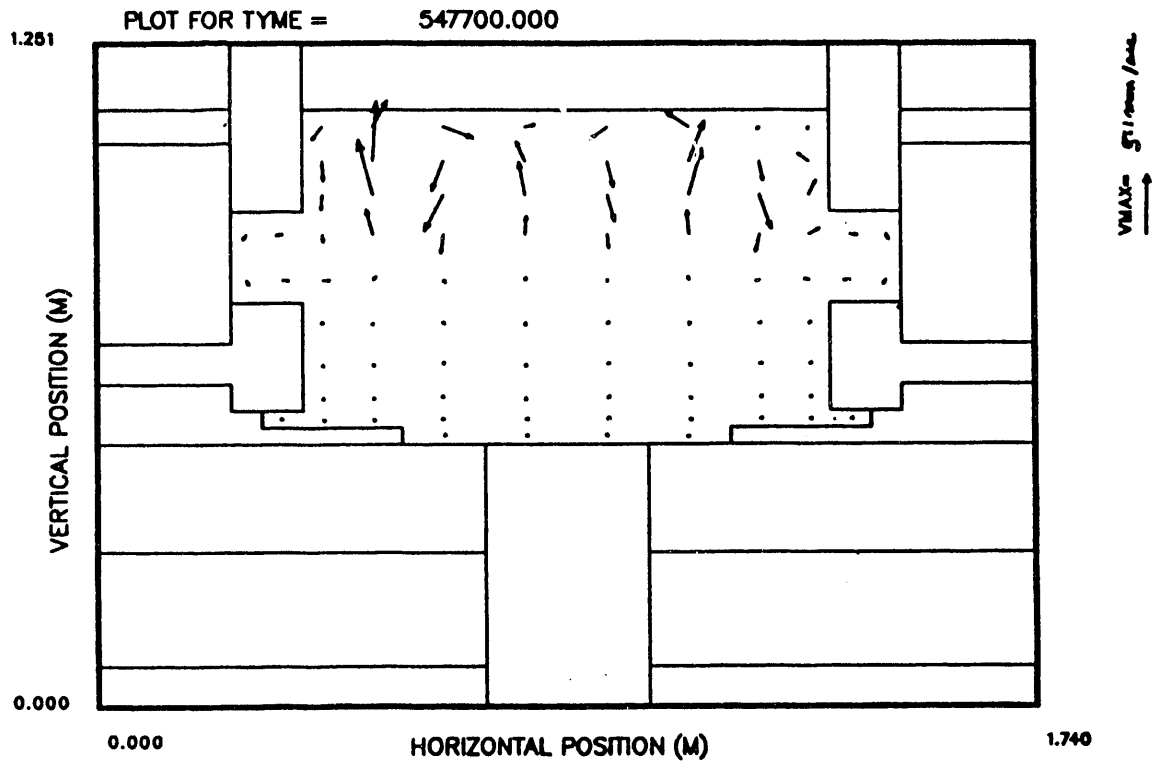0.000   HORIZONTAL POSITION (M)   1.740

FIGURE A.1. Convective Flow Field at t = 152 Hours, PNL
                Simulation Results, from Attachment to Ref.1.

TABLE A.3 **View Factors for Plenum Radiative Heat Transfer**

F_{ij}	3-component		4-component	
	SGM	DWPF	SGM	DWPF
F_{11}	0.000	0.000	0.000	0.000
F_{12}	0.057	0.043	0.057	0.043
F_{21}	0.220	0.276	0.220	0.276
F_{13}	0.772	0.656	0.220	0.364
F_{31}	0.178	0.185	0.220	0.318
F_{14}	–	–	0.552	0.292
F_{41}	–	–	0.166	0.121
F_{22}	0.040	0.025	0.040	0.025
F_{23}	0.660	0.587	0.265	0.329
F_{32}	0.040	0.026	0.069	0.045
F_{33}	0.662	0.607	0.000	0.000
F_{24}	–	–	0.395	0.258
F_{42}	–	–	0.031	0.017
F_{34}	–	–	0.504	0.322
F_{43}	–	–	0.150	0.153
F_{44}	–	–	0.560	0.590

TABLE A.4. Estimated Values of Parameters in Eqs.5 and 6

Parameter	SGM	DWPF
δ_1 (in)	4.25	4.25
ρ_1 (g/cm^3)	2.66	2.66
ρ_3 (g/cm^3)	3.11	3.07
C_{p1} (cal/g.°C)	0.27	0.27
C_{p3} (cal/g.°C)	0.25	0.25
n	3.0	5.5
β_1	0.0467	0.0707
β_3	0.0328	0.0428

END

DATE FILMED
4 / 3 / 93